Hindawi Publishing Corporation
Advances in Civil Engineering
Volume 2015, Article ID 631726, 12 pages
http://dx.doi.org/10.1155/2015/631726

Research Article

Experimental Study of Hysteretic Steel Damper for Energy Dissipation Capacity

Daniel R. Teruna,[1] Taksiah A. Majid,[2] and Bambang Budiono[3]

[1]*Department of Civil Engineering, University of Sumatera Utara, Medan, Indonesia*
[2]*Disaster Research Nexus, School of Civil Engineering, Universiti Sains Malaysia, Penang, Malaysia*
[3]*Department of Civil Engineering, Bandung Institute of Technology, Bandung, Indonesia*

Correspondence should be addressed to Daniel R. Teruna; danielteruna@yahoo.com

Received 8 November 2014; Accepted 2 January 2015

Academic Editor: Andreas Kappos

This study aims to evaluate energy absorption capacity of hysteretic steel damper for earthquake protection of structures. These types of steel dampers are fabricated from mild steel plate with different geometrical shapes on the side part, namely, straight, concave, and convex shapes. The performance of the proposed device was verified experimentally by a series of tests under increasing in-plane cyclic load. The overall test results indicated that the proposed steel dampers have similar hysteretic curves, but the specimen with convex-shaped side not only showed stable hysteretic behavior but also showed excellent energy dissipation capabilities and ductility factor. Furthermore, the load-deformation relation of these steel dampers can be decomposed into three parts, namely, skeleton curve, Bauschinger part, and elastic unloading part. The skeleton curve is commonly used to obtain the main parameters, which describe the behavior of steel damper, namely, yield strength, elastic stiffness, and postyield stiffness ratio. Moreover, the effective stiffness, effective damping ratio, cumulative plastic strain energy, and cumulative ductility factor were also derived from the results. Finally, an approximation trilinear hysteretic model was developed based on skeleton curve obtained from experimental results.

1. Introduction

Conventional design concepts of earthquake-resistant structures are not intended to avoid damage on the structures but to ensure safety of humans under severe earthquakes. However, damage caused by extremely strong earthquakes can result in significant economic impact and loss of human life. Thus, for important or specific purpose of buildings, designing the structural experience with minor damage or elastic response during its life time is necessary. To achieve this goal, structural control systems have been developed and incorporated into structures to minimize or reduce damage induced by wind and earthquakes [1, 2]. Among these systems, passive control system, also known as passive energy dissipation, is an inexpensive and effective way to reduce structural deformation during earthquakes. Passive control systems absorb energy induced by earthquake in various mechanisms, such as metal yielding, friction, fluid orificing, and viscous elastic deformation of solid.

After the Hyogoken-Nanbu earthquake, implementation of passive damper in Japan has significantly increased [3, 4]. In addition, in other areas, such as USA, Asia, and Europe, the application of these systems, either for new buildings or for retrofitting, has been given significant attention [5–9]. Hysteretic steel damper is a passive damper system that absorbs substantial portion of input energy induced by earthquake through hysteretic deformation of the damper material. In the past 20 years, a number of innovative hysteretic steel dampers with high energy dissipation capacity have been proposed and tested, such as Tadas device [10–12], ADAS device [11, 13], honeycomb damper [14], shear panel [15, 16], rhombic ADAS [17, 18], dual-function DFMD [19], slit damper [20–22], buckling restrained brace [23, 24], tube-in-tube damper [25], and circular plate damper [26]. Figure 1 shows several shapes of hysteretic steel dampers. These devices are commonly designed to be incorporated into bracing system of structural frame (Figure 2).

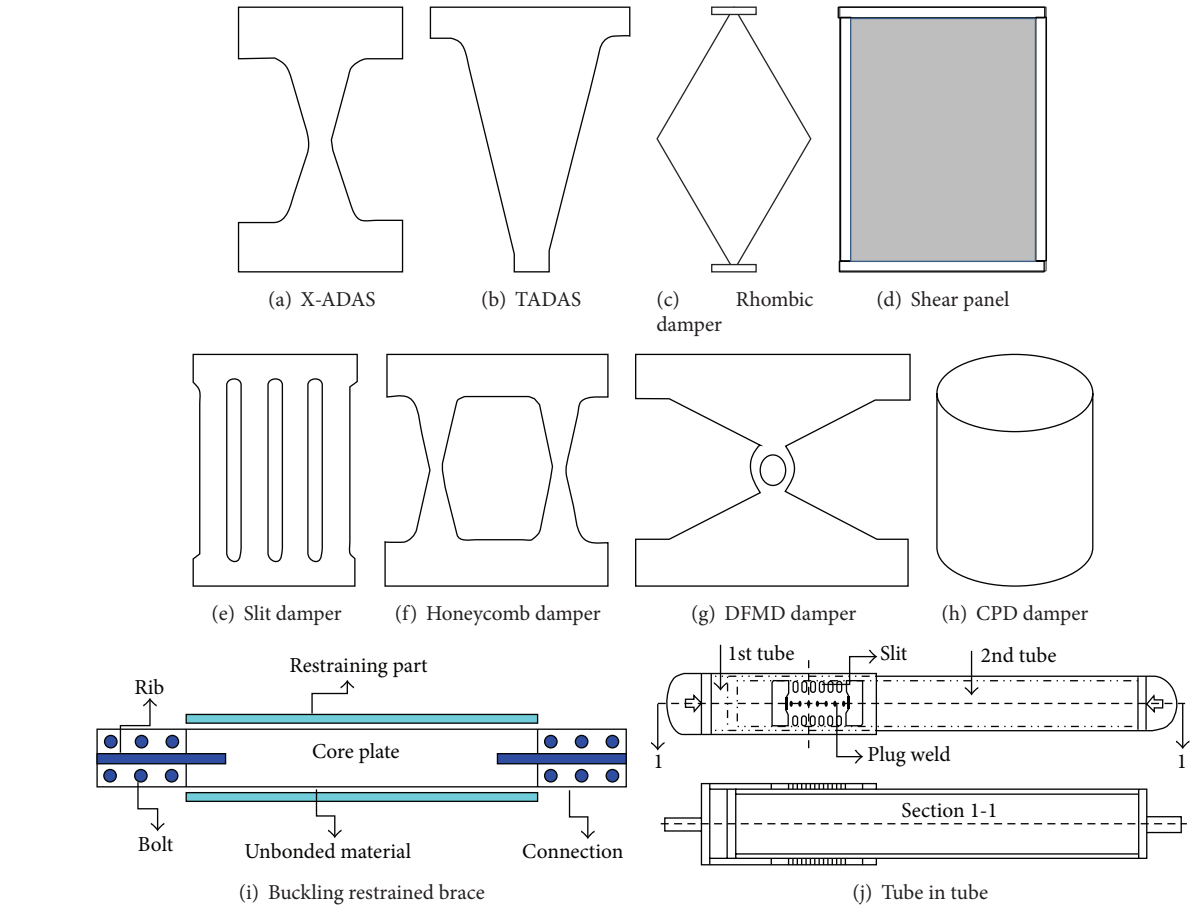

Figure 1: Type of hysteretic steel damper.

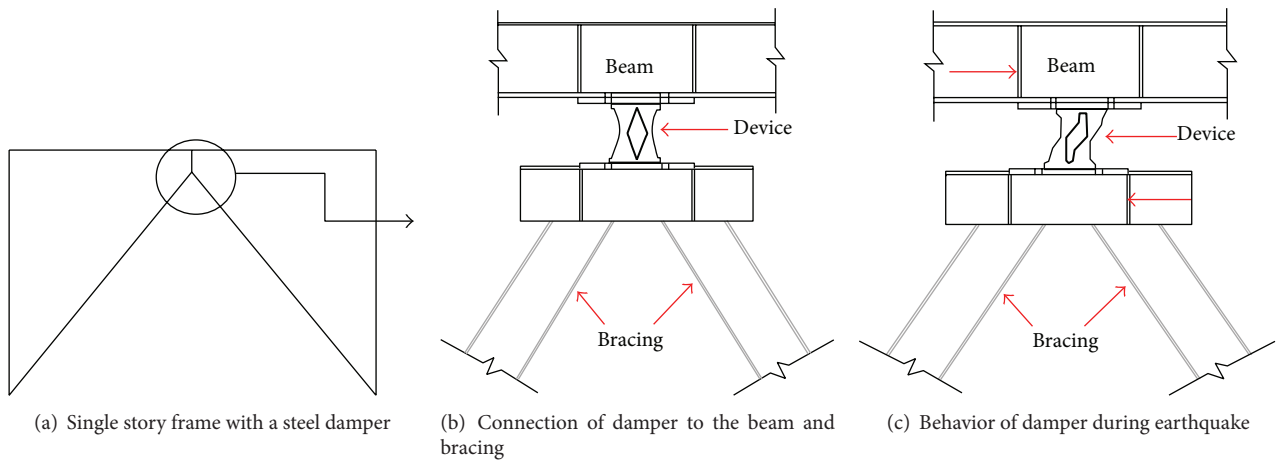

(a) Single story frame with a steel damper

(b) Connection of damper to the beam and bracing

(c) Behavior of damper during earthquake

Figure 2: Typical installation of steel damper in chevron configuration.

Hysteretic steel damper can be classified into three types based on yielding mechanisms, namely, axial, shear, and flexural. ADAS, TADAS, honeycomb device, dual-function DFMD, low-yield rhombic, and slit damper devices belong to the flexure yielding type, whereas buckling-restrained brace systems yield through axial force arising in the braces. Buckling restrained brace systems, which has three parts, namely, steel core element to withstand entire brace axial load, steel tube element filled with mortar for providing confinement that prevents steel core buckling in compression and allows it to yield in tension or compression, and unbounded material placed between steel core and mortar to minimize

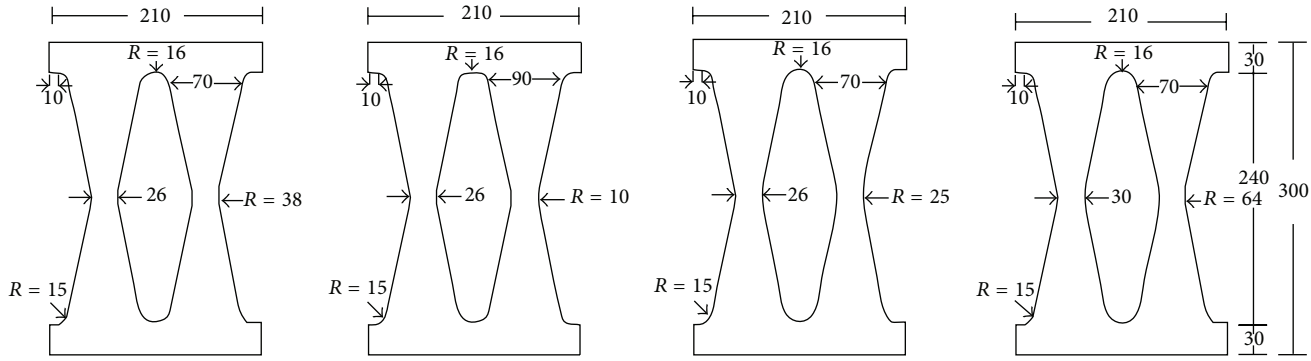

(a) DHSD-1 (b) DHSD-2 (c) DHSD-3 (d) DHSD-4

Figure 3: Details of test specimens.

friction between them. In addition, the tube-in-tube damper proposed by Benavent-Climent [25] consists of outer and inner tubes assembled in two hollow sections using plug and filled weld. The wall of short outer tube has a series of strips made by cutting the wall to form a number of slits. Energy dissipation occurs when slits deform inelastically, which is similar to slit damper. Thus, this damper is a combination of buckling-restrained brace and slit damper.

Flexural yielding dampers assume that under cyclic loading, damper yielding occurs simultaneously and uniformly through the full height of damper, so that it can sustain a large deformation without premature fracture or buckling. However, given that the section properties of slit damper have uniform moment of inertia, yielding is concentrated at both ends under combination of shear force and moment. This concentration is particularly undesirable both in terms of the amount of energy that can be absorbed and by its inherent lack of stability and repeatability in the plastic hinge region.

Furthermore, ADAS, TADAS, and rhombic damper are commonly installed in the direction of weak axis bending to provide energy absorption, whereas the other dampers (honeycomb, dual function DFMD, shear panel, and slit damper) absorb input energy of earthquakes in the direction of strong axis. Therefore, these dampers have a higher stiffness compared with ADAS or TADAS.

2. Objective of the Research

Hysteretic steel dampers of flexural yielding type, such as honeycomb damper, slit damper, and DFMD, which are installed to withstand shear force and bending moment under in plane bending, are not truly yielding simultaneously over the entire plate because the bending moment capacity of the plate is a function of the plate width to the second power; meanwhile, the bending moment diagram is approximately linear. In addition, information about the mechanical characteristics, such as elastic stiffness, yield strength, and postyield stiffness, with regard to hysteretic model for such dampers is limited. The hysteretic model is important for designing earthquake-resistant buildings equipped with steel damper. Thus, further studies are needed to determine the geometrical shapes of steel dampers, which are good and stable in energy dissipation. In this study, four steel damper specimens were made from mild steel plate and fabricated with specific geometry (Figure 3). The steel plates are round in their ends to avoid stress concentration. The tests were performed in the Structural Laboratory of Bandung Institute of Technology. The aim of the test is to determine which among the four proposed dampers has large energy absorption capabilities, stable hysteresis loop, and adequate stiffness.

3. Experimental Program

3.1. Specimens and Loading History. A total of four specimens with specific geometry were fabricated in Mechanical Laboratory of Bandung Institute of Technology using CNC machine to obtain accurate shape and dimensions. The specimens were designated as DHSD1, DHSD2, DHSD3, and DHSD4. All of these specimens have the same width (210 mm), height (300 mm), and thickness (20 mm). The difference between them entirely lies on the shapes of their sides; DHSD1 shows straight side, DHSD2 has concave side, and DHSD3 and DHSD4 were fabricated with convex-shaped sides. The difference between DHSD1 and DHSD2 solely lies in the width at the middle of the specimen, where DHSD3 and DHSD4 have 26 mm and 30 mm width, respectively.

The specimens were welded along the upper and lower steel plates of 40 mm thick, forming similar I-section. Both of these steel plates were designed to be thicker the than specimens to prevent yield when the specimens reached its maximum load or unstable condition. The four specimens were subjected to a displacement amplitude loading pattern (Figure 4). Three cycles were repeated for each displacement amplitude from 1 mm to 20 mm and then followed by two cycles for the next displacement amplitude. The tests were performed until the complete failure of specimens or when the specimens show out-of-plane deformation.

3.2. Material Properties. The specimens were made from mild steel plate with specifications that conform to JIS-SS400. To determine the mechanical characteristics of the material, three tensile coupon tests were conducted (Figure 5 and Table 1 for test results). All specimens and coupon tests were

Table 1: Tensile test results.

Sample	Yield stress (MPa)	Yield strain (10^{-6})	Tensile strength (MPa)	Modulus of elasticity (MPa)	Elongation (%)
20 mm SS400	292	1420	456	2.06×10^5	16

Table 2: Summary of test results.

Specimen	δ_y (mm)	P_y (kN)	K_e (kN/mm)	P_{max}	P_{min}	δ_{max}	δ_{min}	μ
HSD 1	2.5	114.408	45.763	220.11	−212.17	46.5	−46.1	18.6
HSD 2	3.4	139.048	40.896	185.31	−176.54	33.9	−32.7	10.0
HSD 3	3.4	175.90	51.74	274.16	−261.18	47.0	−45.1	14.7
HSD 4	2.6	135.048	51.941	238.09	−245.85	50.0	−50.0	19.2

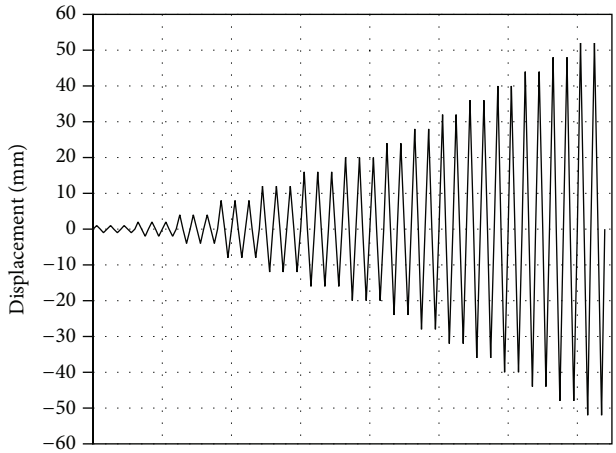

Figure 4: Loading displacement history.

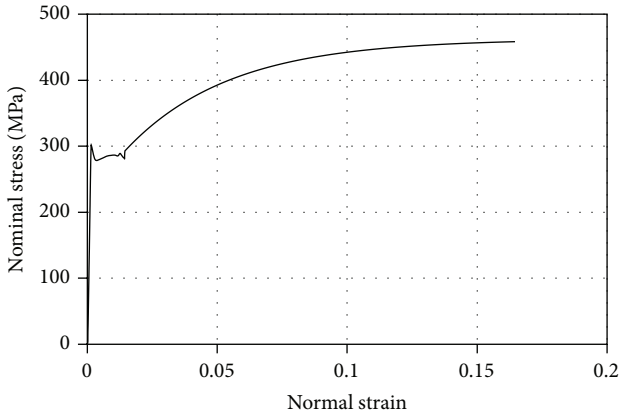

Figure 5: Nominal stress-strain of a test coupon.

taken from the same steel plate sheet in order to minimize the variability of its mechanical properties.

3.3. Test Setup and Measurement. Figure 6 shows the loading setup. The specimen was installed between the strong base frame and upper loading T-beam using high-strength bolts so that the strong axis of specimen is in the direction of applied load. The friction forces between the connected plates caused by the pretension force when the high-strength bolts were tightened had sufficient strength so that the connection would not slip until the specimens reach their maximum strengths. An 800 kN actuator was used to apply the cyclic increasing load to the specimen via the T-beam. To prevent the T-beam from out-of-plane deflection, lateral support with roller was provided and connected to the T-beam. However, the T-beam can rotate on the upper plate of the specimen. Figure 7 presents the photograph of the connection between T-beam and upper plate of specimen while the lateral support systems are shown in Figure 8. The tests were performed until complete failure of the specimens. The failure criterion of the specimens is defined when either a crack appears on the surface or the specimens experience out-of-plane deformation caused by inelastic buckling. The magnitude of the applied load was monitored using a load cell, whereas lateral displacement of specimen and slip between connected parts were measured independently with the use of four sets of displacement transducers (LVDT). LVDT 1 intended to measure the deformation of base support, whereas LVDT 2 measures the slip between bottom plate and base support; no slip occurred during the test. LVDT 3 was used to record the absolute displacement at the upper plate of specimen. The difference measurement of LVDT 3 and LVDT 2 was assumed as lateral displacement of specimen. LVDT 4 was used to control the displacement from actuator. No slip occurred between T-beam and upper plate of specimen because the displacement recorded at LVDT 3 is similar to LVDT 4.

4. Test Results and Discussion

4.1. Hysteretic Behavior. In general, all of the specimens show similar features on the hysteretic behavior without any sign of degradation in both stiffness and strength, except for specimen DHSD-3. All of the specimens deformed in double curvature as expected. The overall test results of four specimens are listed in Table 2. The maximum peak strength P_{max} or P_{min} obtained reached between 1.33x and 1.92x the yield strength because of strain hardening, except for specimen DHSD-3. In addition, the positive peak strength value P_{max} and negative peak strength value P_{min} are not equal because of the Bauchinger effect; however, the differences were <5%. The specimen DHSD-4 also showed the highest ductility and the highest initial stiffness. By contrast, the

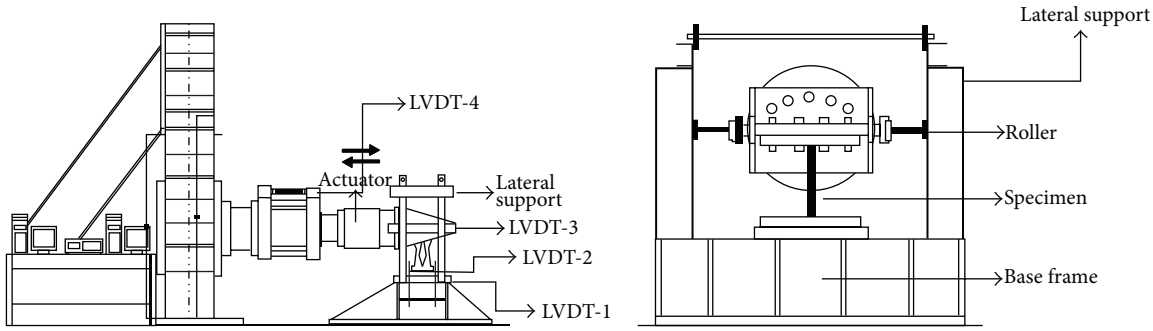

(a) Side view (b) Front view

Figure 6: Test equipment.

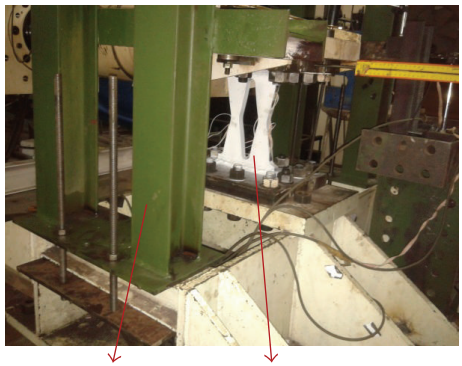

Figure 7: Front view of experimental setup.

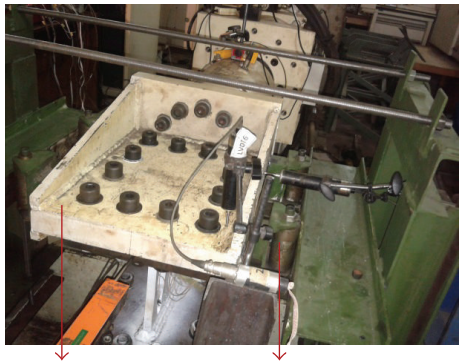

Figure 8: Top view of experimental setup.

specimen DHSD-3 showed the lowest corresponding values. The test results of the four specimens are discussed and summarized in the following sections.

4.1.1. Specimen DHSD-1. The photographs of the specimen before and after testing and its hysteretic curve are shown in Figure 9. The specimen yielded at small displacement and exhibited stable hysteretic behavior. The yielding started at approximately 114 kN applied force. The tests were terminated after the crack appeared on the side vicinity, one-fourth from the top of the specimen height, and the load sustained was reduced. The test results indicate that the geometrical feature of specimen HDSD-1 can be used as damper. However, the specimen DHSD-1 has energy absorption capacity that is lower than that of DHSD-4.

4.1.2. Specimen DHSD-2. Figure 10(a) shows the photograph of specimen DHSD-2. During the test, the specimen shows slight degradation either in stiffness or in strength, and it was also incapable of sustaining a large displacement. When a horizontal force reached 139 kN, yielding started and the test was stopped when the specimen showed out-of-plane deformation at amplitude displacement <33 mm. The specimen buckled because of flexural inelastic buckling (Figure 10(b)). This specimen demonstrates not only less energy dissipation capabilities but also less ductility. Therefore, the geometry of this specimen is not suitable for usage as a hysteretic steel damper.

4.1.3. Specimen DHSD-3. The photograph of specimen DHSD-3 is shown in Figure 11(a). The hysteresis curve obtained from the test is depicted in Figure 11(c). This specimen has both high initial stiffness and energy dissipation capacity. An initial yielding was observed at 179 kN horizontal force. Figure 11(b) shows that the specimen started experiencing out-of-plane bending deformation after testing when the amplitude is equal to 44 mm. The test was terminated when the amplitude increased to 48 mm. However, its overall cyclic behavior is better than that of specimen DHSD-2. The author believes that the out-of-plane inelastic buckling should not occur since this specimen has the similar geometrical shape with DHSD-4. It was probably that this specimen experienced not only in-plane bending but also out-of-plane bending due to the out of straightness either during fabricated or during installation unavoidable. Therefore, further investigation is needed to explain this behaviour. However, the geometrical shape of this specimen is good promising.

4.1.4. Specimen DHSD-4. The photograph of specimen DHSD-4 is shown in Figure 12(a). This specimen can sustain a large amplitude displacement. The yielding started at a horizontal force of 135 kN. The tests were terminated when crack occurred in the region slightly below the top of the

(a) Specimen shape

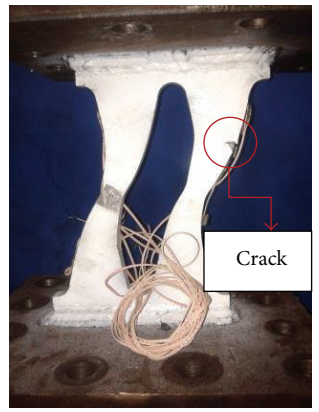

(b) Specimen at failure

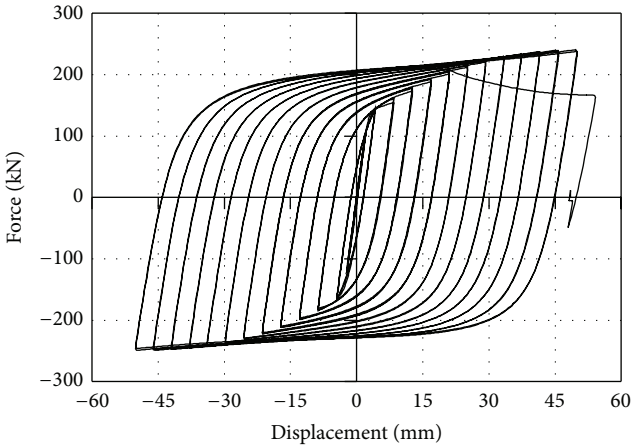

(c) Hysteresis loop

Figure 9: Results of specimen cyclic test for DHSD-1.

(a) Specimen shape

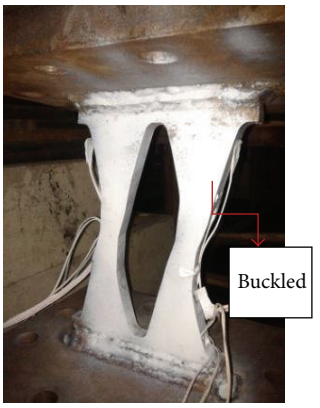

(b) Specimen at failure

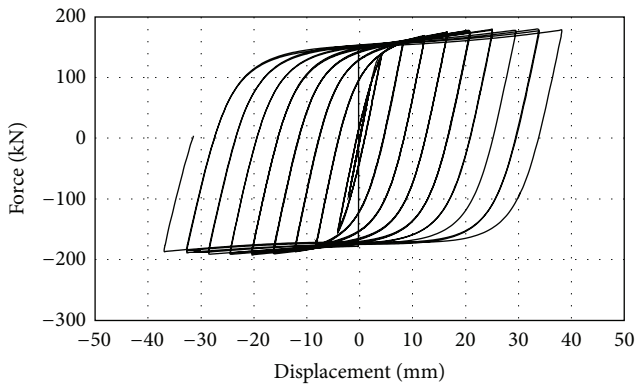

(c) Hysteresis loop

Figure 10: Results of specimen cyclic test for DHSD-2.

(a) Specimen shape

(b) Specimen at failure

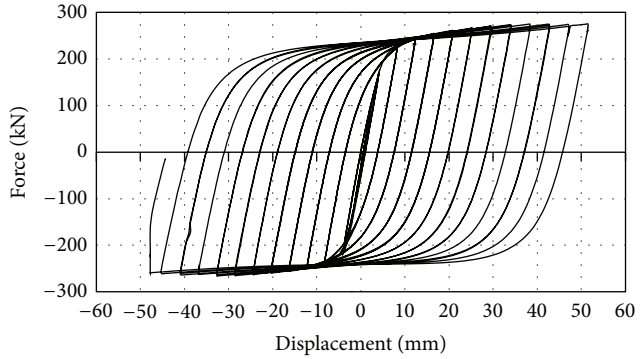

(c) Hysteresis loop

Figure 11: Results of specimen cyclic test for DHSD-3.

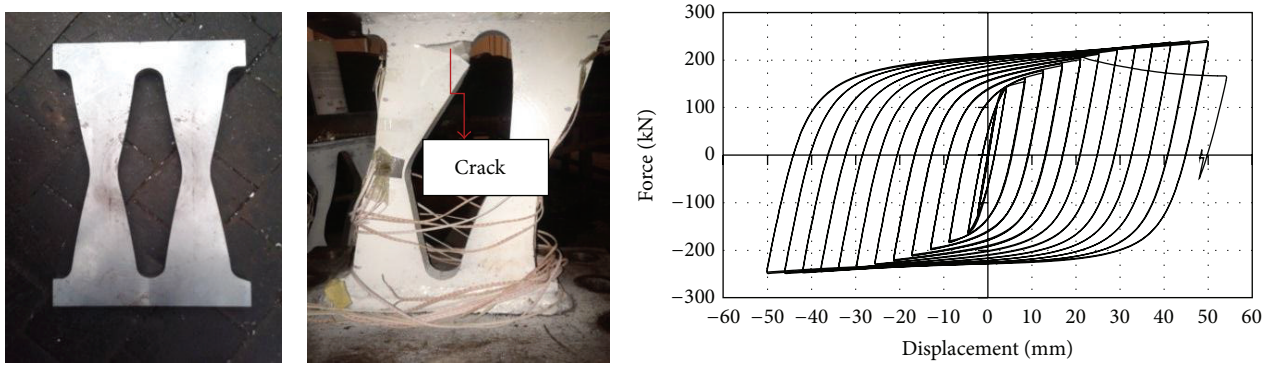

(a) Specimen shape (b) Specimen at failure (c) Hysteresis loop

FIGURE 12: Results of specimen cyclic test for DHSD-4.

specimen. The location of the crack coincides with the region where the maximum bending moment occurred. The experimental results reveal that the specimen with convex-shaped sides exhibits not only excellent energy capacity, but also high elastic stiffness. After testing, no significant distortion was observed and free of undesirable pinching effect. On the basis of the energy dissipation capabilities and cumulative ductility factor, this specimen demonstrates superior performance compared with the other specimens. Therefore, the geometrical shape of this specimen is highly recommended.

4.2. Energy Absorption Capacity. The energy absorption capacity of hysteretic steel damper depends on loading history applied [27]. To study this dependency, the typical stress-strain relation of steel material under cyclic loading can be decomposed into three parts, namely, skeleton, Bauschinger, and elastic unloading (Figure 13). This decomposition is useful for describing hysteretic behavior of structural steel, whereas skeleton part is similar to the stress-strain relation of tensile coupon test under monotonic loading [28]. As shown in Figure 13(b), segments 0-1, 5-6, 11-12, and 17-18 in the positive loading and segments 2-3, 8-9, 14-15, and 20-21 in the negative loading are the paths wherein the load level is larger than the preceding cycle in the same domain. Skeleton curves were obtained by connecting these segments sequentially (Figure 13(c)). The rest of the curve is divided into elastic unloading curves, which have slope close to initial elastic stiffness and Bauschinger curve. The latter curve is softened by the Bauschinger effect.

Plastic energy dissipated by the steel component in each loading until failure can be expressed as the sum of its skeleton and Bauschinger parts as follows:

$$W_D = W_S + W_B, \tag{1}$$

where W_D is total plastic energy dissipation of steel component, W_S, and W_B is total plastic energy dissipation in both positive and negative domains of the skeleton and Baucshinger parts, respectively. Equation (1) can be expressed in normalized form as follows:

$$\eta = {}_S\eta + {}_B\eta,$$
$$\eta = \frac{W_D}{P_y\delta_y}; \quad {}_S\eta = \frac{W_S}{P_y\delta_y}; \quad {}_B\eta = \frac{W_B}{P_y\delta_y}, \tag{2}$$

where P_y is the yield strength; δ_y is the yield displacement; η is equivalent cumulative plastic deformation ratio; ${}_S\eta$ and ${}_B\eta$ are equivalent cumulative plastic deformation ratio of the skeleton and Baushinger parts, respectively. The equivalent cumulative plastic deformation ratio or energy absorption rate η is also known as the index parameter that is commonly used in the energy-based damage model [29]. Moreover, Benavent-Climent [30] proposed energy based damage model using two parameters, namely, the total dissipated energy and the portion of the energy consumed on the skeleton part. It was found that the proposed model can predict level of damage accurately.

Another interest parameter is recognized as cumulative ductility factor ${}_\mu\eta$ which is defined as

$${}_\mu\eta = \left|{}_\mu\eta^+\right| + \left|{}_\mu\eta^-\right| = \frac{\left|{}_S\delta^+\right| + \left|{}_S\delta^-\right|}{\delta_y}, \tag{3}$$

where ${}_S\delta^+$and ${}_S\delta^-$ are the apparent cumulative plastic deformation ratio on the skeleton part in the positive and negative regions. Table 3 shows the cumulative ductility factor, the equivalent cumulative plastic deformation ratio of the specimens η, and that of both skeleton curve (${}_S\eta$) and Bauschinger part (${}_B\eta$). In general, energy consumed by Bauschinger part is >80% of the total plastic energy. Figure 14 also shows the relation between cumulative energy dissipated and cumulative displacements of four specimens data obtained from cumulative energy dissipated and ductility displacement of the four specimens; the specimen DHSD-4 shows the largest energy dissipation capacity, whereas in terms of cumulative ductility factor, specimen DHSD-1 is almost equal to specimen DHSD-4.

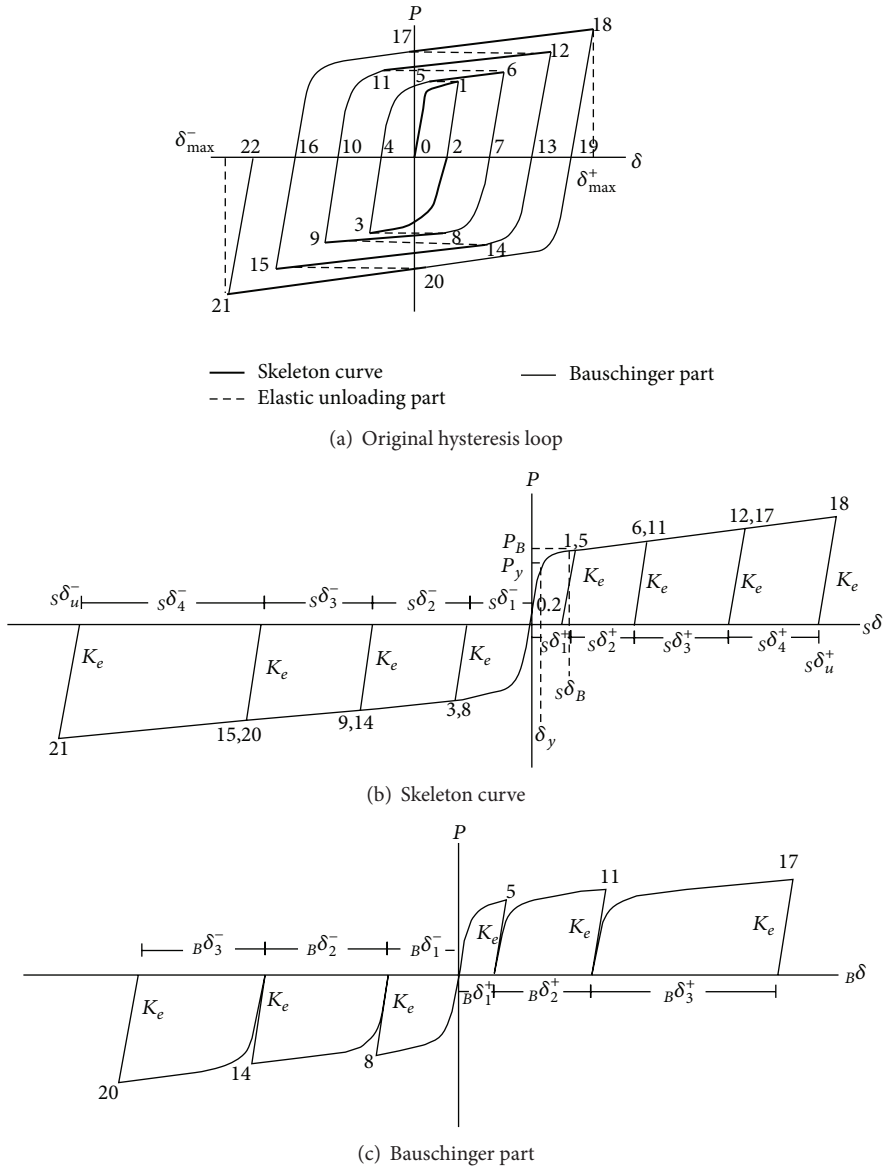

Figure 13: Decomposition of hysteresis loop.

4.3. Effective Stiffness and Effective Damping. Analysis of the response of the structures with linear dynamic procedure requires effective stiffness and effective damping. Figure 15 illustrates the physical significance of the effective stiffness and may be calculated as follows:

$$K_{\text{eff}} = \frac{\left|P^{+}\right| + \left|P^{-}\right|}{\left|\delta^{+}\right| + \left|\delta^{-}\right|}. \tag{4}$$

The energy dissipation capability of hysteretic system is generally represented by effective damping ζ, whereas effective damping is displacement-dependent and calculated at design displacement, δ, as follows [31]:

$$\zeta_{\text{eff}} = \frac{1}{2\pi}\left[\frac{W_D}{K_{\text{eff}}\delta^2}\right], \tag{5}$$

where W_D is the energy dissipated per cycle, which is obtained from the test and equal to the area enclosed by one complete cycle of the force-displacement relation of hysteresis loop. Table 4 presents effective stiffness and effective damping for the four specimens calculated at the maximum displacement. The relation between effective damping and displacement at every cycle are shown in Figure 16.

Table 5 presents the damping coefficients as function of effective damping (FEMA 273). The damping coefficients are useful for reducing ordinary spectral response acceleration through coefficients B_s and B_1 as specified by numerous building code. The average damping ratio provided by steel damper specimens at displacement 20 mm (assumption of interstory drift target for building structures remain elastic) is >40%. Therefore, the use of steel damper can protect

Table 3: Energy dissipation capacity.

Specimen	${}_S\eta$	${}_B\eta$	η	${}_S\eta/\eta$	${}_B\eta/\eta$	${}_\mu\eta$
DHSD-1	22218.24	131533.04	153751.28	0.145	0.855	50.20
DHSD-2	23972.02	211257.82	235229.82	0.102	0.898	30.57
DHSD-3	16139.40	68693.55	84832.95	0.190	0.809	23.35
DHSD-4	25451.86	214267.43	239719.29	0.106	0.894	49.93

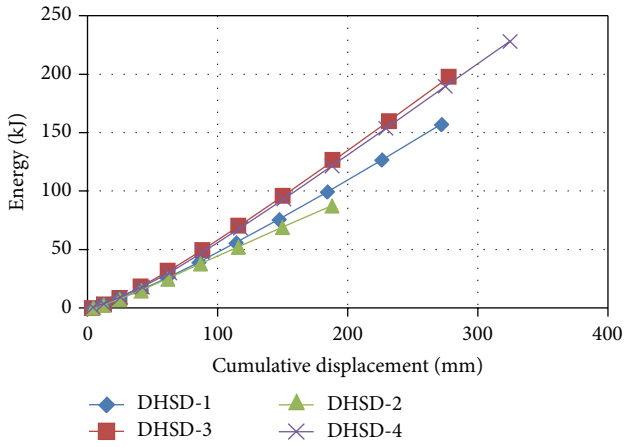

Figure 14: Cumulative energy dissipation of the specimens.

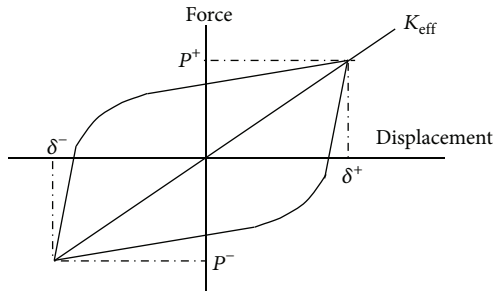

Figure 15: Definition of effective stiffness.

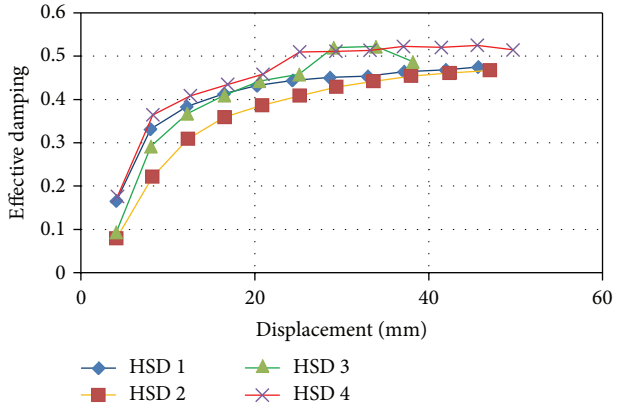

Figure 16: Effective damping ratio versus displacement.

Table 4: Effective damping and stiffness at maximum displacement.

Specimens	Effective damping ζ (%)	Effective stiffness (kN/mm)
DHSD-1	0.475	4.668
DHSD-2	0.467	5.433
DHSD-3	0.487	5.812
DHSD-4	0.512	4.839

Table 5: Damping coefficient.

Effective damping ζ (percentage of critical)	B_s	B_1
5	1	1
10	1.3	1.2
20	1.8	1.5
30	2.3	1.7
40	2.7	1.9
50	3.0	2.0

a structure should it remain elastic or experience minor damage under severe seismic excitation.

4.4. Approximate Trilinear Model. Previous studies proposed hysteretic models of steel damper, such as the bilinear model [32], trilinear model A [25], two-surface model [1], Boug-Wen [33], modified Boug-Wen [18], and Ramberg-Osgood [15], based on either experimental or numerical results. In the present study, a trilinear model is adopted to characterize the parameters involved in the development of force-deformation relationship of the damper because of its simplicity and this type of model is available in the commercial software package. Figure 17 shows the comparison of trilinear model and skeleton curve for the four specimens, whereas the mechanical properties of approximate trilinear model of the specimens are listed in Table 6. α_1 and α_2 are the ratios of elastic stiffness to the first and the second plastic stiffness, respectively.

5. Conclusion and Future Researches

5.1. Conclusion. This paper presented some experiments on the energy dissipation capabilities of the yielding steel damper under in-plane cyclic loading. The conclusions are summarized as follows.

(1) All of the specimens exhibit stable hysteretic behavior under moderate displacement; however, specimen

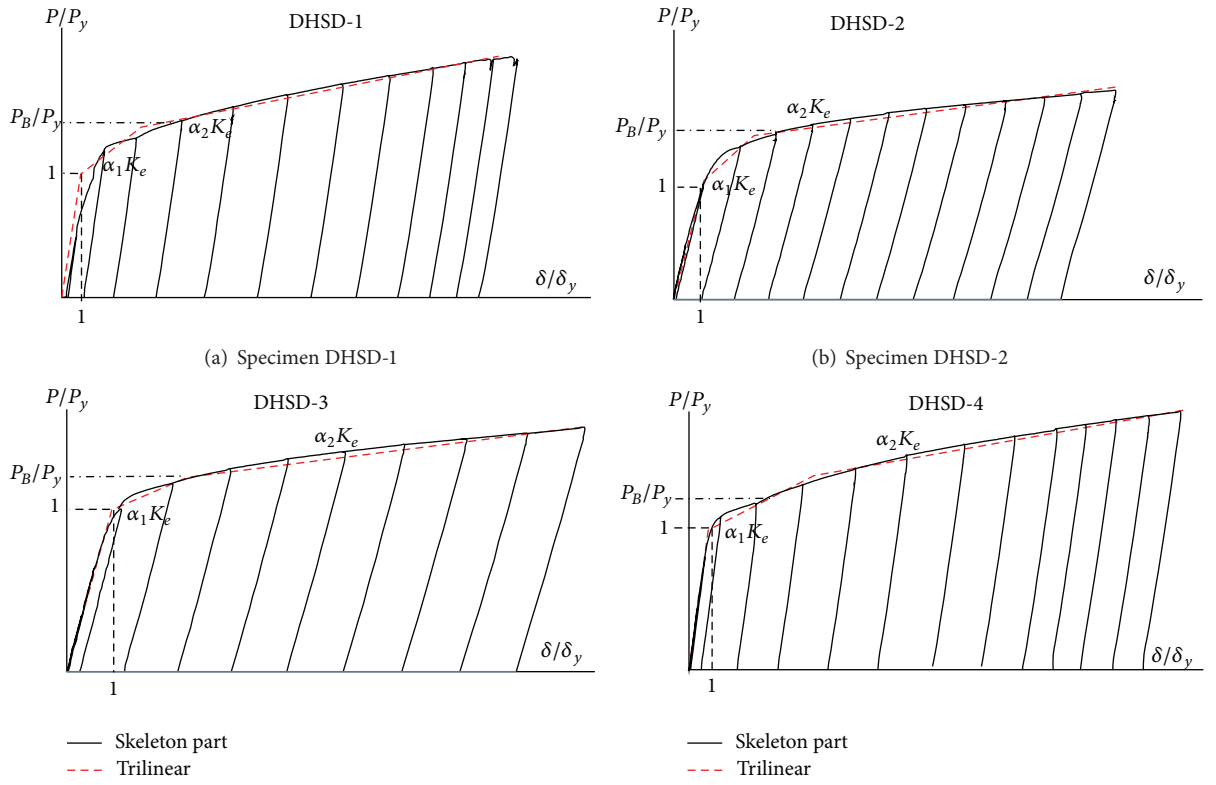

Figure 17: Comparison of skeleton curve and trilinear approximation.

Table 6: Mechanical characteristic of trilinear approximation.

Specimen	δ_y	P_y	(P_B/P_y)	K_{p1}	K_{p2}	$\alpha 1\ (K_{p1}/K_e)$	$\alpha 2\ (K_{p2}/K_e)$
HSD 1	2.5	114.408	1.379	5.419	1.387	0.118	0.030
HSD 2	3.4	139.048	1.2	4.855	1.438	0.118	0.035
HSD 3	3.4	175.9	1.380	11.708	1.751	0.226	0.033
HSD 4	2.6	135.048	1.391	3.668	1.257	0.070	0.024

DHSD-3 showed slight decrease in stiffness and strength under large displacement because of the lack of stability.

(2) Average energy consumed by Baushinger part of specimens is >80% of the total plastic energy.

(3) On the basis of evaluation using the four indexes, namely, elastic stiffness, ductility factor, cumulative ductility factor, and energy absorption rate, specimen DHSD-4 demonstrated superior performance compared with other specimens.

(4) The specimens showed >40% hysteretic damping ratio under moderate displacement, whereas the maximum hysteretic damping ratio of >50% was achieved by specimen DHSD-4 at maximum displacement.

(5) The skeleton curves of the specimens can be approximated using trilinear model using parameters elastic stiffness, yield force, and the first and second postyield stiffness.

5.2. Future Researches. With this study investigation of hysteretic steel damper under cyclic loads has been conducted and it would be desirable to undertake the further research in the following areas:

(1) To perform a parametric study of the damper with convex side to obtain the effect of height-width ratio on the hysteretic behavior of the dampers.

(2) To investigate the effect of out of straightness on the hysteretic behavior of the damper with various height-width ratio and thickness to height or width ratio.

(3) To investigate the lack of damper stability before cracking occurred at maximum displacement as expected.

(4) To developed mathematical formulation on the mechanical characteristic dampers, especially elastic stiffness of the damper for application of the trilinear hysteretic model.

Conflict of Interests

The authors declare that there is no conflict of interests regarding the publication of this paper.

Acknowledgments

This research was funded by the Ministry of Higher Education of Indonesia and University of Sumatera Utara Medan, Indonesia (Grant no. 4267/UNS.1.R/KEU/2013).

References

[1] G. F. Dargush and T. T. Soong, "Behavior of metallic plate dampers in seismic passive energy dissipation systems," *Earthquake Spectra*, vol. 11, no. 4, pp. 545–568, 1995.

[2] T. T. Soong and B. F. Spencer Jr., "Supplemental energy dissipation: state-of-the-art and state-of-the-practice," *Engineering Structures*, vol. 24, no. 3, pp. 243–259, 2002.

[3] A. Wada, Y. H. Huang, and M. Iwata, "Passive damping technology for buildings in Japan," *Progress in Structural Engineering and Materials*, vol. 2, pp. 335–350, 2000.

[4] H. Kamura, K. Nanba, K. Oki, and T. Funaba, "Seismic response control for high-rise buildings using energy-dissipation devices," JFE Technical Report 14, 2009.

[5] M. D. Symans, F. A. Charney, A. S. Whittaker et al., "Energy dissipation systems for seismic applications: current practice and recent developments," *Journal of Structural Engineering*, vol. 134, no. 1, pp. 3–21, 2008.

[6] K. Miyamoto, A. Gilani, L. Determan, and R. Hanson, "Design of an essential facilities with steel moment frame and viscous damper using NEHRP procedure," in *Proceedings of the 13th World Conference on Earthquake Engineering*, Vancouver, Canada, 2004.

[7] D. M. Aniello, C. G. Della, and F. M. Mazzolani, "'All-steel' buckling restrained braces for seismic upgrading of existing reinforced buildings," in *Proceedings of the 6th International Conference on Behavior of Steel Structures in Seismic Areas (STESSA '09)*, Philadelphia, Pa, USA, 2009.

[8] K. C. Chang, J. S. Hwang, and S. N. Lee, "Status of application of passive control technologies in Taiwan," in *Proceedings of the 13th World Conference on Earthquake Engineering*, Vancouver, Canada, 2004.

[9] Q. Xie, "State of the art of buckling-restrained braces in Asia," *Journal of Constructional Steel Research*, vol. 61, no. 6, pp. 727–748, 2005.

[10] A. S. Whittaker, V. V. Bertero, J. L. Alonso, and C. L. Thompson, "Earthquake simulator testing of steel plate added damping and stiffness elements," Report UCB/EERC-89/02, University of California, Berkeley, Calif, USA, 1989.

[11] A. S. Whittaker, V. V. Bertero, C. L. Thompson, and L. J. Alonso, "Seismic testing of steel plate energy dissipation devices," *Earthquake Spectra*, vol. 7, no. 4, pp. 563–604, 1991.

[12] K. C. Tsai, H. W. Chen, C. P. Hong, and Y. F. Su, "Design of steel triangular plate energy absorbers for seismic-resistant construction," *Earthquake Spectra*, vol. 9, no. 3, pp. 505–528, 1993.

[13] M. D. Bergman and C. S. Goel, "Evaluation of cyclic testing of steel plate devices for added damping and stiffness," Report UMCE 87-10, 1987.

[14] T. Kobori, Y. Miura, E. Fukusawa et al., "Development and application of hysteresis steel dampers," in *Proceedings of the 10th World Conference on Earthquake Engineering*, pp. 2341–2346, 1992.

[15] M. Nakashima, "Strain-hardening behavior of shear panels made of low-yield steel. I: test," *Journal of structural Engineering*, vol. 121, no. 12, pp. 1742–1749, 1995.

[16] D. Foti, M. Diaferio, and R. Nobile, "Optimal design of a new seismic passive protection device made in aluminium and steel," *Structural Engineering and Mechanics*, vol. 35, no. 1, pp. 119–122, 2010.

[17] M.-H. Shih, W.-P. Sung, and C.-G. Go, "Investigation of newly developed added damping and stiffness device with low yield strength steel," *Journal of Zhejiang University Science*, vol. 5, no. 3, pp. 326–334, 2004.

[18] M.-H. Shih and W.-P. Sung, "A model for hysteretic behavior of rhombic low yield strength steel added damping and stiffness," *Computers and Structures*, vol. 83, no. 12-13, pp. 895–908, 2005.

[19] G. Li and H. Li, "Earthquake-resistant design of RC frame with 'dual functions' metallic dampers," in *Proceedings of the 14th World Conference on Earthquake Engineering*, Beijing, China, 2008.

[20] H. M. Lee, H. S. Oh, C. Huh, S. Y. Oh, H. M. Yoon, and S. T. Moon, "Ultimate energy absorption capacity of steel plate slit dampers subjected to shear force," *Steel Structures*, vol. 2, pp. 71–79, 2002.

[21] S. H. Oh, Y. J. Kim, and H. S. Ryu, "Seismic performance of steel structures with slit dampers," *Engineering Structures*, vol. 31, no. 9, pp. 1997–2008, 2009.

[22] R. W. K. Chan and F. Albermani, "Experimental study of steel slit damper for passive energy dissipation," *Engineering Structures*, vol. 30, no. 4, pp. 1058–1066, 2008.

[23] M. Iwata, "Application design of buckling restrained braces in Japan," in *Proceedings of the 13th World Conference on Earthquake Engineering*, Vancouver, Canada, 2004.

[24] M. Iwata and M. Murai, "Buckling-restrained brace using steel mortar planks; performance evaluation as a hysteretic damper," *Earthquake Engineering and Structural Dynamics*, vol. 35, no. 14, pp. 1807–1826, 2006.

[25] A. Benavent-Climent, "A brace-type seismic damper based on yielding the walls of hollow structural sections," *Engineering Structures*, vol. 32, no. 4, pp. 1113–1122, 2010.

[26] D. Y. Abebe, J. W. Kim, and J. H. Choi, "Hysteresis characteristic of circular pipe steel damper using LYP 225," in *Proceedings of the Steel Innovation Conference*, Christchurch, New Zealand, 2013.

[27] Y. Jiao, Y. Shimada, S. Kishiki, and S. Yamada, "Study of energy dissipation capacity of steel beams under cyclic loading," in *Proceedings of the 6th International Conference on Behavior of Steel Structures in Seismic Areas (STESSA '09)*, Philadelphia, Pa, USA, 2009.

[28] S. Yamada, M. Yamaguchi, T. Takeuchi, and A. Wada, "Hysteresis model of steel material for the bucklingrestrained brace considering the strain rate dependency," in *Proceedings of the 13th World Conference on Earthquake Engineering (WCEE '04)*, Vancouver, Canada, August 2004.

[29] Y. J. Park and A. H. S. Ang, "Mechanistic seismic damage model for reinforced concrete," *Journal of Structural Engineering*, vol. 111, no. 4, pp. 722–739, 1985.

[30] A. Benavent-Climent, "An energy-based damage model for seismic response of steel structures," *Earthquake Engineering and Structural Dynamics*, vol. 36, no. 8, pp. 1049–1064, 2007.

[31] A. K. Chopra, *Dynamics of Structures: Theory and Applications to Earthquake Engineering*, Pearson—Prentice Hall, 3rd edition, 1995.

[32] C. Xia and R. D. Hanson, "Influence of ADAS element parameters on building seismic response," *Journal of Structural Engineering (ASCE)*, vol. 118, no. 7, pp. 1903–1918, 1992.

[33] J. C. De la Llera, C. Esguerra, and J. L. Almazán, "Earthquake behavior of structures with copper energy dissipators," *Earthquake Engineering and Structural Dynamics*, vol. 33, no. 3, pp. 329–358, 2004.